Gain-Scheduled and Linear Parameter-Varying Approaches in Control of Active Magnetic Bearings

Alexander Smirnov[1,a], Rafal P. Jastrzebski[1,b], Katja M. Hynunen[1,c]
[1]Lappeenranta University of Technology, 53851, P.O.Box 20, Finland
[a]Alexander.Smirnov@lut.fi, [b]Rafal.Jastrzebski@lut.fi, [c]Katja.Hynunen@lut.fi

Abstract: In this paper Linear Parameter Varying, gain-scheduled and robust approaches for a controller synthesis are considered in an application for a highly gyroscopic system. A transient during a rotor start up and a steady state disturbance attenuation are evaluated. Based on these measurements a comparison of different control approaches is done.

Keywords: Linear Parameter Varying, LPV, Robust Control, Gain-Scheduled Control, Gyroscopic System

Introduction

Active magnetic bearings are intended to remove a friction of the rotor by levitating it with the help of magnetic forces. In that way maintenance requirements are significantly reduced.

The main challenge for an AMB system is to control the levitation. Electromagnets can provide only attractive forces, so the system is in the position of unstable equilibrium or open-loop unstable.

Different control techniques can be applied to stabilize the system. The industry mostly adopts PID controllers due to their simplicity [1]. This simple technique leads to the decen-tralized control. A more beneficial way is to use Linear Quadratic Gaussian (LQG),H_∞ or μ controllers that take into account coupling between rotor ends and coupling between planes due to the gyroscopic effect.

Controllers in AMB systems should have good robustness properties. This results from the sensitivity of the system to uncertainties. There can be different sources of uncertainties, such as variations of rotor bending frequencies, structural resonances, actuator nonlinearities, and imprecise measurements. One of the major sources of uncertainty in the magnetic bearing system is a rotational speed. The linear system model is usually derived for a certain rotational speed and a deviation from that speed causes the uncertainty.

To solve this problem a gain-scheduled controllers are applied. A separate controller for each speed interval is synthesized with a tuned model. During the operation controllers are switched according to the measured rotational speed.

The direct switch introduces a bump in control signal and undesired overshoot in the rotor position. One way is to implement a bumpless transfer, but it introduces an additional compu-tational burden. For each controller a special feedback should be calculated to keep the output signals of the off-line controller similar to the signals of the on-line one. The second way is to use an interpolation technique. In that way we are restricted to the controllers of the same

structure and order. The gain-scheduled approach was implemented for an AMB system by Matsumura [2].

The most significant disadvantage of the mentioned gain-scheduled techniques is the absence of a possibility to guarantee robustness. Actually the system is subjected to the requirement of slow varying parameters. Therefore, under the rapid changes of the rotor speed the system can go unstable.

A method inspired by gain-scheduling and without its drawbacks is a Linear Parameter Varying (LPV) approach. It provides a consistent framework for controller synthesis under parameter variations. As in most cases the rotor speed is available for measurements, the AMB is a perfect application for that technique.

A LPV controller for an AMB system was investigated in the literature [3]. However the used model of the magnetic bearing system was relatively simple and did not explicitly include any flexible modes of the rotor.

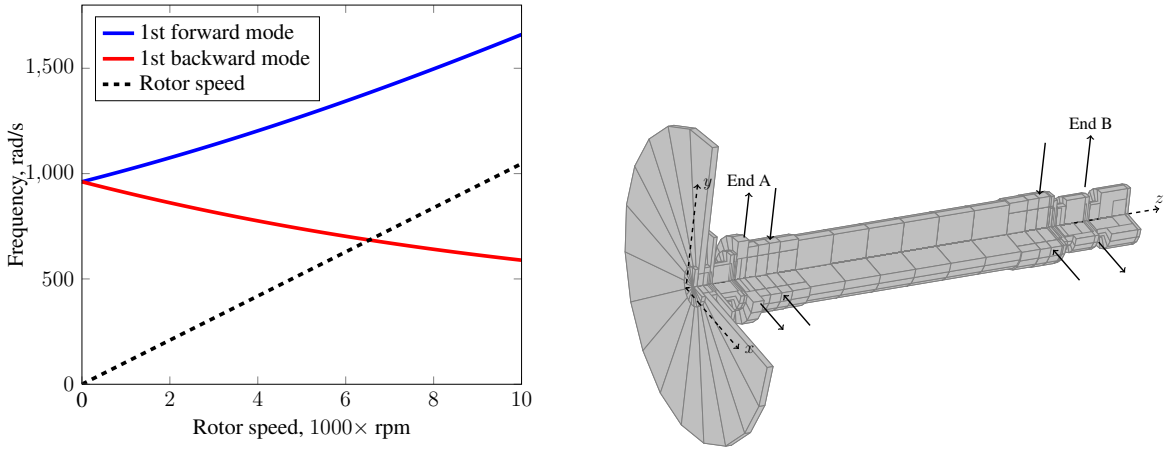

(a) Campbell diagram

(b) Rotor FEM model

Figure 1: Rotor model

The flexible modes are a source of a significant uncertainty in the system that is not easily reduced by the feedback control [4]. They usually require a special attention and techniques to make the system operate in a super critical region. The problem is more complicated as the flexible modes tends to split and change their frequency with the rotor speed. An example of splitting the first flexible mode is presented in Figure 1a.

In this work a common interpolation technique is compared with a more sophisticated LPV approach. Typical gain-scheduled controllers showed sufficient performance and robustness. They were able to stabilize the plant over all frequency range in cases where LQG and $\mathcal{H}_\infty$ controllers failed [5].

AMB System Modeling

The equations of motion for the rotor are based on the Finite Element Method (FEM) solution. A dynamic system is composed with the use of Lagrange's equations as described by Chen and Gunter [6].

The system is presented with four inputs and four outputs. Inputs are the currents of the electromagnets $[i_{\mathrm{Ax}}\ i_{\mathrm{Ay}}\ i_{\mathrm{Bx}}\ i_{\mathrm{By}}]$ on both sides of the rotor. The outputs are the positions $[x_{\mathrm{A}}\ y_{\mathrm{A}}\ x_{\mathrm{B}}\ y_{\mathrm{B}}]$ measured by eddy current sensors.

Along with a rigid body motion bending modes are also considered. The first one lies in the actuator bandwidth so it is used in the model for a controller synthesis.

The model is build in the relation to the coordinates of the center of mass $\mathbf{x}_\mathrm{c}^T = [x\ y\ \alpha\ \beta]$. Each flexible mode adds two additional coordinates, displacements in x and y directions. The full vector of the linear rotor model with the first flexible mode has 12 states, coordinates themselves and their first derivatives $\mathbf{x}_\mathrm{r}^T = [x_\mathrm{c}\ \dot{x}_\mathrm{c}]$. The LPV form of the rotor model can be written as following

$$\begin{aligned}\dot{\mathbf{x}} &= \mathbf{A}_\mathrm{r}(\Omega)\mathbf{x}_\mathrm{r} + \mathbf{B}_\mathrm{r}\mathbf{u},\\ \mathbf{y}_\mathrm{r} &= \mathbf{C}_\mathrm{r}\mathbf{x}_\mathrm{r}.\end{aligned} \tag{1}$$

In the described system the matrix $\mathbf{A}_\mathrm{r}$ is the only one that depends on a scheduled parameter Ω. This parameter is the rotor rotational speed and is measured in real time.

The common approach is to linearize the system around operational point with the help of bias currents [7]

$$f_\mathrm{x} = \frac{\mu_0 N^2 S_\mathrm{air}\cos\chi}{4}\left(\left(\frac{i_\mathrm{bias}+i_\mathrm{c}}{l_0-x}\right)^2 - \left(\frac{i_\mathrm{bias}-i_\mathrm{c}}{l_0+x}\right)^2\right). \tag{2}$$

Thus a non-linear relation of a current and a magnetic force (2) becomes a linear one

$$f_\mathrm{x} = k_\mathrm{i} i_\mathrm{c} + k_\mathrm{x} x, \tag{3}$$

$$k_\mathrm{i} = \frac{\partial f}{\partial i_\mathrm{c}}\Big|_{x=0,i_\mathrm{c}=0} = \frac{\mu_0 N^2 S_\mathrm{air} i_\mathrm{bias}\cos\chi}{l_0^2}, \tag{4}$$

$$k_\mathrm{x} = \frac{\partial f}{\partial i_\mathrm{c}}\Big|_{x=0,i_\mathrm{c}=0} = \frac{\mu_0 N^2 S_\mathrm{air} i_\mathrm{bias}^2\cos\chi}{l_0^3}. \tag{5}$$

Current k_i and position k_x stiffnesses are obtained as in equations (4) and (5). In the system model these stiffnesses are included into each input channel resulting in 4×4 diagonal matrices

$$\mathbf{K}_\mathrm{i} = \begin{bmatrix} k_\mathrm{i} & 0 & 0 & 0\\ 0 & k_\mathrm{i} & 0 & 0\\ 0 & 0 & k_\mathrm{i} & 0\\ 0 & 0 & 0 & k_\mathrm{i}\end{bmatrix} \quad \mathbf{K}_\mathrm{x} = \begin{bmatrix} k_\mathrm{x} & 0 & 0 & 0\\ 0 & k_\mathrm{x} & 0 & 0\\ 0 & 0 & k_\mathrm{x} & 0\\ 0 & 0 & 0 & k_\mathrm{x}\end{bmatrix}. \tag{6}$$

The state-space matrices (1) are obtained as

$$\mathbf{A}_\mathrm{r} = \begin{bmatrix} \mathbf{0} & \mathbf{I}\\ -\mathbf{M}_\mathrm{r}^{-1}\left(\mathbf{K}_\mathrm{r} - \mathbf{C}_\mathrm{f}^T\mathbf{K}_\mathrm{x}\mathbf{C}_\mathrm{f}\right) & -\mathbf{M}_\mathrm{r}^{-1}\left(\mathbf{D}_\mathrm{r} + \Omega\mathbf{G}_\mathrm{r}\right)\end{bmatrix} \quad \mathbf{B}_\mathrm{r} = \begin{bmatrix}\mathbf{0}\\ -\mathbf{M}_\mathrm{r}^{-1}\mathbf{C}_\mathrm{f}^T\mathbf{K}_\mathrm{i}\end{bmatrix},$$
$$\mathbf{C}_\mathrm{r} = \begin{bmatrix}\mathbf{C}_\mathbf{x} & \mathbf{0}.\end{bmatrix} \tag{7}$$

The gyroscopic matrix $\mathbf{G}_\mathrm{r}$, the damping matrix $\mathbf{D}_\mathrm{r}$, the stiffness matrix $\mathbf{K}_\mathrm{r}$, and the mass matrix $\mathbf{M}_\mathrm{r}$ describe the rotor dynamics. The coupling with electromagnets is provided by current and position stiffnesses, transformed to the rotor coordinates with transformation matrix $\mathbf{C}_\mathrm{f}$.

The inner structure of the matrices is presented as follows

$$\mathbf{G}_\mathrm{r} = \begin{bmatrix} 0 & 0 & 0 & 0 & 0 & 0\\ 0 & 0 & 0 & 0 & 0 & 0\\ 0 & 0 & 0 & I_\mathrm{d} & I_\mathrm{d1} & 0\\ 0 & 0 & -I_\mathrm{d} & 0 & 0 & I_\mathrm{d1}\\ 0 & 0 & -I_\mathrm{d1} & 0 & 0 & I_\mathrm{d2}\\ 0 & 0 & 0 & -I_\mathrm{d1} & -I_\mathrm{d2} & 0\end{bmatrix}, \tag{8}$$

$$\mathbf{M}_\mathrm{r} = \mathrm{diag}(m,\ m,\ I_x,\ I_y,\ m_f,\ m_f), \tag{9}$$

$$\mathbf{D}_\mathrm{r} = \mathrm{diag}(0,\ 0,\ 0,\ 0,\ d_f,\ d_f), \tag{10}$$

$$\mathbf{K}_\mathrm{r} = \mathrm{diag}(k_m,\ k_m,\ k_I,\ k_I,\ k_f,\ k_f). \tag{11}$$

The $\mathrm{diag}()$ term stands for the matrix with elements inside the round brackets placed on the main diagonal.

The transformation matrices $\mathbf{C_x}$ and $\mathbf{C_f}$ transform the rotor coordinates to the displacement at the sensor positions and outer forces to the rotor coordinates at the actuator positions, respectively

$$\mathbf{C_x} = \begin{bmatrix} 1 & 0 & 0 & -l_{\mathrm{s,A}} & l_{\mathrm{s,f1,A}} & 0 \\ 0 & 1 & l_{\mathrm{s,A}} & 0 & 0 & l_{\mathrm{s,f1,A}} \\ 1 & 0 & 0 & l_{\mathrm{s,B}} & -l_{\mathrm{s,f1,B}} & 0 \\ 0 & 1 & -l_{\mathrm{s,B}} & 0 & 0 & -l_{\mathrm{s,f1,B}} \end{bmatrix}, \tag{12}$$

$$\mathbf{C_f} = \begin{bmatrix} 1 & 0 & 0 & -l_{\mathrm{a,A}} & l_{\mathrm{a,f1,A}} & 0 \\ 0 & 1 & l_{\mathrm{a,A}} & 0 & 0 & l_{\mathrm{a,f1,A}} \\ 1 & 0 & 0 & l_{\mathrm{a,B}} & -l_{\mathrm{a,f1,B}} & 0 \\ 0 & 1 & -l_{\mathrm{a,B}} & 0 & 0 & -l_{\mathrm{a,f1,B}} \end{bmatrix}. \tag{13}$$

In addition it is important to include an actuator dynamics. The delay of the actuator is approximated by the first order transfer function in each channel. The resulting state-space matrices are

$$\begin{aligned} \mathbf{A}_{\mathrm{a}} &= \mathrm{diag}(-W_{\mathrm{bw}},\ -W_{\mathrm{bw}},\ -W_{\mathrm{bw}},\ -W_{\mathrm{bw}}), \\ \mathbf{B}_{\mathrm{a}} &= \mathrm{diag}(W_{\mathrm{bw}},\ W_{\mathrm{bw}},\ W_{\mathrm{bw}},\ W_{\mathrm{bw}}), \\ \mathbf{C}_{\mathrm{a}} &= \mathbf{I}_{4\times 4}. \end{aligned} \tag{14}$$

The resulting equations for the full system which combines rotor and actuator have the following form

$$\begin{aligned} \mathbf{A} &= \begin{bmatrix} \mathbf{A}_{\mathrm{a}} & \mathbf{0} \\ \mathbf{B}_{\mathrm{r}}\mathbf{C}_{\mathrm{a}} & \mathbf{A}_{\mathrm{r}} \end{bmatrix} \quad \mathbf{B} = \begin{bmatrix} \mathbf{B}_{\mathrm{a}} \\ \mathbf{0} \end{bmatrix}, \\ \mathbf{C} &= \begin{bmatrix} \mathbf{0} & \mathbf{C}_{\mathrm{r}} \end{bmatrix}. \end{aligned} \tag{15}$$

All the mentioned parameters are listed in Table 1.

Controller Synthesis

The idea of Linear Parameter Varying controller originates from a gain-scheduled technique. The main difference between gain-scheduled and LPV controllers is that the first can utilize the non-linear description of the system while the second relies on the LPV representation.

The gain-scheduled controller uses the available in real-time information of the current operational point of the system to switch to the controller synthesized to that particular point or to the closest one to the point. Eventually an idea of interpolating controllers between points was utilized. Later several authors addressed a problem of synthesizing a controller directly instead of constructing from a family of controllers, resulting in the LPV design. A good review with a historical insight is given by Leith in his work [8].

The LPV approach became popular in last decades and is intensively studied. The problem can be formulated in the several ways. One is based on a parameter-dependent quadratic Lyapunov function [9], in the second the problem is presented as a special robust performance problem, where special weights and a plant structure are used. Later in the literature a framework that unifies these two methods was introduced [10].

In this work all types of controllers are based on $\mathcal{H}_\infty$ approach. There are no restrictions on other approaches but unified basis allows to provide a comprehensive comparison between controllers.

Table 1: List of parameters

Parameter	Value	Description
k_i	268.08 [N/A]	Current stiffness
k_x	992120 [N/m]	Position stiffness
m	73.543 [kg]	Rotor mass
$I_\mathrm{x},\ I_\mathrm{y}$	10.550 [kg·m]	Moments of inertia in x and y directions
m_f	18.069 [kg]	Modal mass of the first flexible mode
d_f	143.05 [N· m/s]	Damping of the first flexible mode
k_m	$2.6584 \cdot 10^{-5}$ [N/m]	Rotor stiffness in x and y directions
k_I	$1.1665 \cdot 10^{-5}$ [N/m]	Rotor stiffness in α and β directions
k_f	$1.6696 \cdot 10^{7}$ [N/m]	Modal stiffness of the first flexible mode
I_d	0.5915 [kg·m]	Diametral moment of inertia
I_d1	3.1505 [kg·m]	Diametral moment of inertia of the first flexible mode
I_d2	18.428 [kg·m]	Diametral moment of inertia of the first flexible mode
$l_\mathrm{s,A}$	0.2519 [m]	Distance from the center of mass to the sensor on the A end
$l_\mathrm{s,B}$	0.6863 [m]	Distance from the center of mass to the sensor on the B end
$l_\mathrm{s,f1,A}$	0.2265 [m]	Modal distance of the flexible mode to the sensor on the A end
$l_\mathrm{s,f1,B}$	0.6021 [m]	Modal distance of the flexible mode to the sensor on the B end
$l_\mathrm{a,A}$	0.1787 [m]	Distance from the center of mass to the actuator on the A end
$l_\mathrm{a,B}$	0.5613 [m]	Distance from the center of mass to the actuator on the B end
$l_\mathrm{a,f1,A}$	0.3802 [m]	Modal distance of the flexible mode to the actuator on the A end
$l_\mathrm{a,f1,B}$	0.2535 [m]	Modal distance of the flexible mode to the actuator on the B end
W_bw	$1.7932 \cdot 10^{3}$ [rad/s]	Bandwidth of an actuator

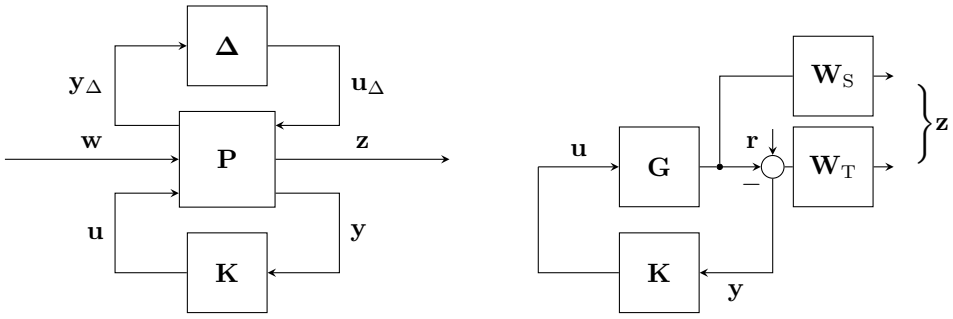

(a) General control configuration (b) Mixed-sensitivity control

Figure 2: Control problems

The general linear $\mathcal{H}_\infty$ problem is to find a controller $\mathbf{K}$ such that it minimizes

$$\|\mathbf{F}_\mathrm{l}(\mathbf{P},\mathbf{K})\|_\infty = \max_\omega \bar{\sigma}(\mathbf{F}_\mathrm{l}(\mathbf{P},\mathbf{K})(j\omega)) \leq \gamma, \tag{16}$$

where $\mathbf{F}_\mathrm{l}$ is a *lower fractional transformation*, $\mathbf{K}$ is a controller, $\bar{\sigma}$ is an upper singular value. The generalized plant $\mathbf{P}$ is obtained from the original plant.

The structured uncertainty is introduced to the system by the block $\mathbf{\Delta}$. The generalized plant $\mathbf{P}$ is weighted according to the common mixed-sensitivity $\mathcal{H}_\infty$ control problem. In this work an S/T scheme is used which is presented in Figure 2b.

To shape the plant to the desired objectives the following weightening functions are used

$$\mathbf{W}_\mathrm{S} = \mathbf{I}_{4\times4} \cdot 0.5\frac{s+144}{s+0.144}, \quad \mathbf{W}_\mathrm{T} = \mathbf{I}_{4\times4} \cdot 0.5\frac{s+0.01}{s+10}. \tag{17}$$

The uncertainty parameter for the $\mathbf{\Delta}$-structure includes only the rotor speed. The other uncertainties can be also included in the same way but that part is out of the scope of the work.

The LPV controller is synthesized using the same structure as in Figure 2a but with the use of a LPV plant described by (1) and (15).

This work uses the approach presented by Apkarian [9]. For each vertex of the system an $\mathcal{H}_\infty$ controller is synthesized using the same Lyapunov function. This insures the stability and performance on the full range of the parameters variation. The final controller is interpolated depending on the measured speed.

Having the state-space matrices for each vertex $\mathbf{A}_\mathrm{K}(\Omega),\ \mathbf{B}_\mathrm{K}(\Omega), \mathbf{C}_\mathrm{K}(\Omega), \mathbf{D}_\mathrm{K}(\Omega)$ the controller for the particular point is obtained as

$$\begin{bmatrix} \mathbf{A}_\mathrm{K}(\Omega) & \mathbf{B}_\mathrm{K}(\Omega) \\ \mathbf{C}_\mathrm{K}(\Omega) & \mathbf{D}_\mathrm{K}(\Omega) \end{bmatrix} = \sum_{i=1}^{r} \alpha_i \begin{bmatrix} \mathbf{A}_{\mathrm{K}i} & \mathbf{B}_{\mathrm{K}i} \\ \mathbf{C}_{\mathrm{K}i} & \mathbf{D}_{\mathrm{K}i} \end{bmatrix}, \tag{18}$$

where α_i is such that

$$\Omega = \left\{ \sum_{i=1}^{r} \alpha_i \omega_i :\ \alpha_i \geq 0,\ \sum_{i=1}^{r} = 1 \right\}. \tag{19}$$

The r denotes the total number of vertices and ω_i the particular vertex. The parameter Ω is measured in real time and the controllers are updated on each step.

Evaluation of controllers

In this work several approaches are used and compared in application to AMB system. The main aim is to stabilize the rotor around the operational point for the full speed range from 0 to $10\ 000$ rpm.

At first the robust $\mathcal{H}_\infty$ controller is synthesized using the mentioned $\mathbf{\Delta}$ structure. The benefit of such a controller is that it does not require the measurements of the rotor speed. It is stable, if possible, for the full range of the uncertain parameter variation.

The second one is an optimal $\mathcal{H}_\infty$ controller. It is obtained for each point of the system and thus does not include an uncertainty or a speed measurements. This type is implemented only for a comparison as it is not feasible in real system to calculate the controller for each point.

The third one is an interpolated $\mathcal{H}_\infty$ controller. It is an interpolation of two controllers which are synthesized for the minimum and maximum rotor speeds. The interpolation is done in the same way as described by (18).

The last one is a LPV controller which was discussed in detail earlier.

Each controller is synthesized using the same weightening functions. As the main objective is the stability of the system, a maximum singular value of sensitivity functions is evaluated. A good starting point for a comparison is an output sensitivity function $\mathbf{S}_\mathrm{o}$ [11]. Additionally an output complementary sensitivity function $\mathbf{T}_\mathrm{o}$ is used for the comparison. These functions are defined as

$$\mathbf{S}_\mathrm{o} = (\mathbf{I} + \mathbf{GK})^{-1}, \tag{20}$$

$$\mathbf{T}_\mathrm{o} = \mathbf{GK}\,(\mathbf{I} + \mathbf{GK})^{-1}. \tag{21}$$

The sensitivity functions are evaluated at each operational point of the plant and a maximum value is calculated. The plant used for the evaluation includes three flexible modes of the rotor. The results are presented in the Figure 3.

In Figure 3a it is seen that the LPV controllers have the lowest norm, thus being the best solution. An important feature of a robust controller can be seen in both Figure 3a and Figure 3b is that the norm stays the same regardless of the uncertainty value. It is obvious that the robust controller to tolerate the uncertainty sacrificed the performance resulting in the high overall norm value.

The optimal controller shows the best achievable point for an output complementary sensitivity function in Figure 3b. In Figure 3a its value is a bit higher than that of a LPV controller.

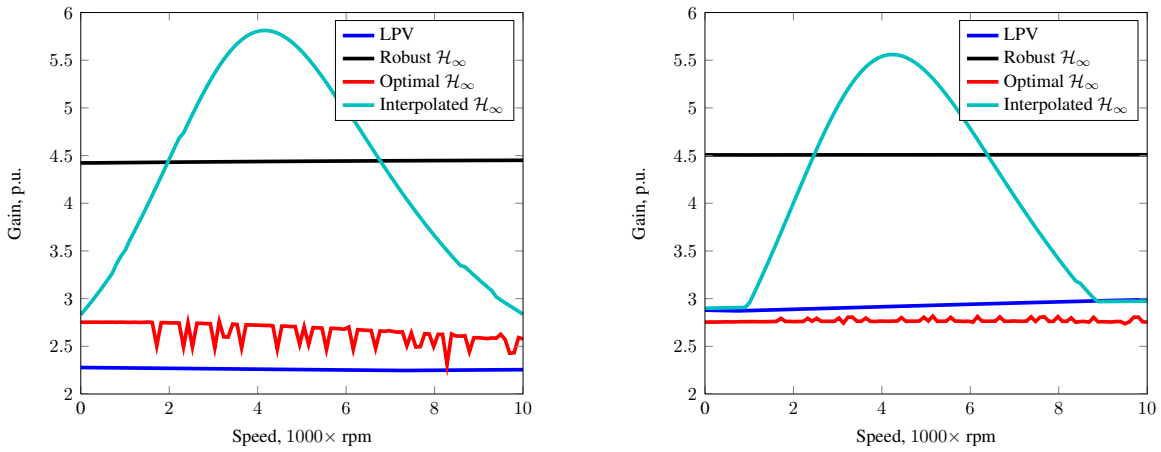

(a) Output sensitivity

(b) Output complementary sensitivity

Figure 3: Maximum values of sensitivity functions

This is the result of the chosen weightening scheme so that the complementary function is more emphasized. Additionally optimal controller shows some oscillations, with a magnitude of 0.5 in the fist case and less than 0.1 in the second. This is a result of the numerical errors.

It is seen that the interpolated controller shows good performance around minimum and maximum points and has the highest value in the midrange. It should be noted that at boundaries the interpolated controller does not reach the optimal one because of the numerical problems. The optimal controller is achieved using a Linear Matrix Inequality (LMI) approach resulting in a minimum point. The interpolated controller is found by using gamma iterations and solving Riccati equations with gamma tolerance of 0.1. When using the LMI approach the interpolated controller experiences the numerical problems resulting in unrealistically high maximum singular values.

The behavior of controllers in Figure 3a and Figure 3b shows that a LPV approach provides the best solution in the sense of stability and disturbance rejection. The interpolated controller can be used only around the points where it has been synthesized. Definitely the uncertainty space can be divided into more pieces thus achieving a performance close to the optimal controller. This is what is usually done to ensure the stability for an interpolated controller.

The sensitivity functions plots tell about closed loop performance of a linear plant around operational point. For further evaluation the nonlinear simulations are carried. For these simulations a system with three flexible modes is used. The force current relations are non-linear; they include actuator delay and are based on look-up tables from the switch-reluctance network model [12].

In the simulation, the rotor accelerates from zero to the maximum speed. The sinusoidal disturbance introduces an unbalance forces in the model. The results are achieved for a robust and LPV controllers, an interpolated controller shows an unstable response while passing the first flexible mode. The displacements at the A end in x direction are presented in Figure 4a and Figure 4b.

The transient responses are quite similar for both controllers. The oscillations with the highest magnitude appear around the backward whirl of the first flexible mode. The system successfully cross the first mode around 6500 rpm, which is shown by the horizontal gray line. For the sake of convenience the rotor speed is plotted in the same figures with the blue dashed line. It can be noted that a LPV controller has a two times greater magnitude of oscillations. These oscillations in both cases are damped in the same time interval.

There is also another point where the system experiences oscillations. It is near the maximum speed and it can be explained by the decceleration of the rotor. The LPV controller has a

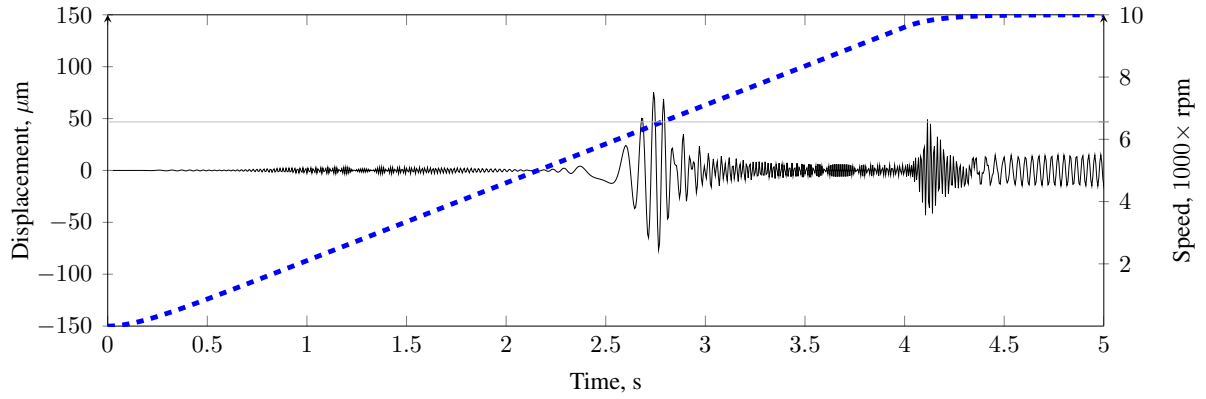

(a) Robust $\mathcal{H}_\infty$ controller

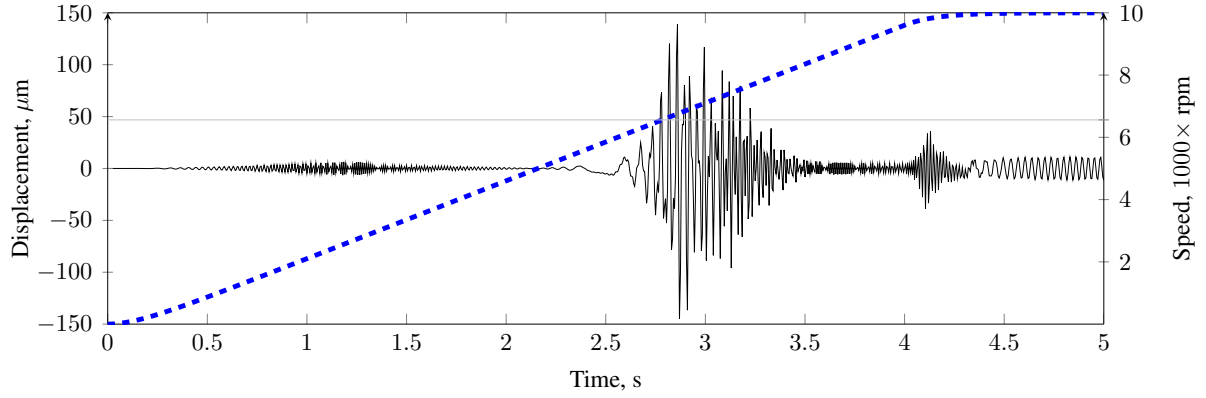

(b) LPV controller

Figure 4: Rotor acceleration responses

lower oscillations magnitude around this point, the difference is 35%.

Such a behavior can be explained by an adaptive nature of a LPV controller. On each step the gains are modified according to the rotational speed. During startup process the system does not have enough time to adapt. This results in a higher amplitude of oscillations.

The speed of a parameter variation is a significant problem for the LPV controllers and usually the main point of conservatism in that approach [8].

There is a totally different picture at the steady state. A disturbance to the x channel of the rotor A-end is applied at the maximum rotational speed. The amplitude is 10% of the maximum current. The simulation results are presented in Figure 5.

It can be seen that at the steady state the robust controller has almost three times larger disturbance response. Another important feature for that controller is a significant coupling between rotor ends. In case of a LPV controller that coupling is almost removed.

Hardware issues. The modern controllers compared to the commonly used PIDs are almost impossible to implement in hardware using analog solutions. Thus a digital implementation is the most popular nowadays [13]. The modern Digital Signal Processors (DSPs) allow achieve a high sampling rate and Field Programmable Gate Arrays (FPGAs) work even faster. Despite these facts the problem of reaching a desired sampling rate with high order controllers still exists.

The most expensive operation in the controller computing on a DSP, omitting an analog-to-digital conversion, is a multiplication. For example in the wide 28x Delfino series of Texas Instruments microcontrollers with floating point unit (FPU) this operation takes 40 ns [14].

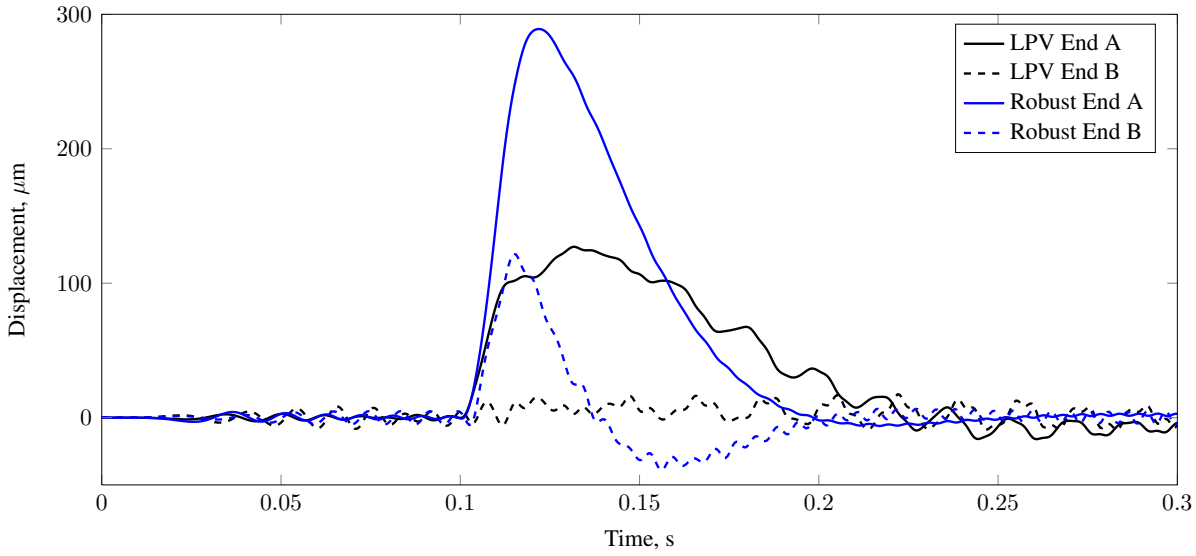

Figure 5: Step disturbance response for controllers in x direction

A linear controller is considered in the state-space form

$$\dot{\mathbf{x}} = \mathbf{A}_{n\times n}\mathbf{x}_{n\times 1} + \mathbf{B}_{n\times i}\mathbf{u}_{i\times 1}, \tag{22}$$

$$\mathbf{y} = \mathbf{C}_{o\times n}\mathbf{x}_{n\times 1} + \mathbf{D}_{o\times i}\mathbf{u}_{i\times 1}. \tag{23}$$

The letters $n,\ i,\ o$ denote the number of states inputs and outputs, respectively. Thus a number of multiplications needed to compute a controller is

$$N = n^3 + n \cdot i^2 + o \cdot n^2 + o \cdot i^2. \tag{24}$$

A typical controller for AMBs has four inputs and four outputs. The robust controller in this work has 24 states. Thus using the formula (24) the total number of multiplications is $16\ 828$. With the mentioned value for the multiplication operation the time consumed by DSP will be $673\ \mu$s, which already exceeds the usual sampling time around $100\ \mu$s. Of course a faster DSP or a FPGA have enough computational power to handle the task.

The LPV controller uses the interpolation scheme (18) thus introducing additionally $n^2 + n \cdot i + o \cdot n + o \cdot i$ multiplication for each vertex. In this work with two vertices it is 1624 multiplications. Which is 10% more and should not cause significant problems.

The interpolated $\mathcal{H}_\infty$ controller showed that two points are not enough to achieve robust and reliable control. The issue can be solved by griding the space into more intervals. Usually tens of points are used. The increase in number of points does not cause an increase in computation time because the interpolation happens only between the two controllers at a time. The requirements for available memory definitely is greater but there is a plenty of memory on modern chips.

When the interval is divided into several parts problems can occur when switching on the boundaries of these parts. It can cause the difference in output signals and thus a bump during the switch. Such a behavior is undesirable especially during the rotor start up. To alleviate a problem various techniques can be used such as presented in [15, 16].

Conclusion

In this work a LPV, an interpolation and a robust control approaches are examined in application for an AMB system. The system with a highly gyroscopic rotor is considered. In this kind of

systems the frequency splitting is a source of a significant uncertainty that is a challenge for control.

From the mentioned controllers the interpolated controller is not able to stabilize the system during the start up process. The solution can be in denser griding of an uncertainty space.

The robust controller showed the best behavior during the rotor acceleration. Thus it can be recommended as a first try in most cases. The drawback is a pure performance at the steady state.

The LPV controller showed a reasonable solution when there are strict requirements at the steady state. The behavior during the start up is worse than that of a robust controller but the values do not exceed the safety margins. The controller synthesis procedure relies on the same problem formulation as a robust controller. Thus it is not a sophisticated problem to extend the system to the one with the LPV approach.

Additionally hardware implementations are discussed. The modern high order controller in conjunction with a high sampling rate required for an AMB system demands a significant computational power. It was shown that the LPV controller requires only 10% more computation time than the robust controller of the same order. The interpolated controller requires the same amount as the LPV, but can cause some problems during the switch. The problems arise when an uncertainty interval is splitted into several parts.

The mentioned results were supplied with analytical analysis and simulation results based on a non-linear model.

References

[1] C. Knospe, "PID control," *Control Systems Magazine, IEEE*, vol. 26, no. 1, pp. 30–31, February 2006.

[2] F. Matsumura, T. Namerikawa, K. Hagiwara, and M. Fujita, "Application of gain scheduled h_∞ robust controllers to a magnetic bearing," *Control Systems Technology, IEEE Transactions on*, vol. 4, no. 5, pp. 484–493, Sep 1996.

[3] B. Lu, H. Choi, G. D. Buckner, and K. Tammi, "Linear parameter-varying techniques for control of a magnetic bearing system," *Control Engineering Practice*, vol. 16, no. 10, pp. 1161 – 1172, 2008.

[4] G. Li, Z. Lin, and P. E. Allaire, "Uncertainty classification for rotor-AMB systems," in *The tenth international symposium on magnetic bearings*, 2006.

[5] R. P. Jastrzebski, K. M. Hynynen, and A. Smirnov, "H[infinity] control of active magnetic suspension," *Mechanical Systems and Signal Processing*, vol. 24, no. 4, pp. 995 – 1006, 2010.

[6] W. J. Chen and E. J. Gunter, *Introduction to dynamics of rotor-bearing systems*. Victoria, B.C.: Trafford Publishing, 2005.

[7] R. Larsonneur, *Magnetic Bearings: Theory, Design, and Application to Rotating Machinery*. Springer Berlin Heidelberg, 2009, ch. 2, pp. 27–68.

[8] D. J. Leith and W. E. Leithead, "Survey of gain-scheduling analysis and design," *International Journal of Control*, vol. 73, no. 11, pp. 1001–1025, July 2000.

[9] P. Apkarian, P. Gahinet, and G. Becker, "Self-scheduled H_∞ control of linear parameter-varying systems: a design example," *Automatica*, vol. 31, no. 9, pp. 1251 – 1261, 1995.

[10] F. Wu, "A generalized lpv system analysis and control synthesis framework," *International Journal of Control*, vol. 74, no. 7, pp. 745–759, 2001.

[11] G. Li, E. H. Maslen, and P. E. Allaire, "A note on ISO AMB stability margin," in *The tenth international symposium on magnetic bearings*, 2006.

[12] J. Nerg and R. Pöllänen, "Modelling the performance characteristics of radial active magnetic bearings: comparison of 2-d and 3-d finite element method and reluctance network method," in *ICC'05: Proceedings of the 9th International Conference on Circuits*. Stevens Point, Wisconsin, USA: World Scientific and Engineering Academy and Society (WSEAS), 2005, pp. 1–6.

[13] R. Larsonneur, *Magnetic Bearings: Theory, Design, and Application to Rotating Machinery*. Springer Berlin Heidelberg, 2009, ch. 9, pp. 229–250.

[14] *TMS320F28335/F28334/F28332/F28235/F28234/F28232 Digital Signal Controllers (Rev. H)*, Web site: [Last accessed: 10.05.2010]. [Online]. Available: http://www.ti.com/lit/gpn/tms320f28335

[15] M. C. Turner and D. J. Walker, "Linear quadratic bumpless transfer," *Automatica*, vol. 36, no. 8, pp. 1089 – 1101, 2000.

[16] J. D. Bendtsen, J. Stoustrup, and K. Trangbaek, "Bumpless transfer between observer-based gain scheduled controllers," *International Journal of Control*, vol. 78, no. 7, pp. 491–504, 2005.